International Journal of Bioorganic Chemistry
2017; 2(3): 135-145
http://www.sciencepublishinggroup.com/j/ijbc
doi: 10.11648/j.ijbc.20170203.19

A Systematic Study of the Biofield Energy Healing Treatment on Physicochemical, Thermal, Structural, and Behavioral Properties of Magnesium Gluconate

Mahendra Kumar Trivedi[1], Alice Branton[1], Dahryn Trivedi[1], Gopal Nayak[1], William Dean Plikerd[1], Peter L. Surguy[1], Robert John Kock[1], Rolando Baptista Piedad[1], Russell Phillip Callas[1], Sakina A. Ansari[1], Sandra Lee Barrett[1], Sara Friedman[1], Steven Lee Christie[1], Su-Mei Chen Liu[1], Susan Elizabeth Starling[1], Susan Jones[1], Susan Mardis Allen[1], Susanne Kathrin Wasmus[1], Terry Ann Benczik[1], Thomas Charles Slade[1], Thomas Orban[1], Victoria L. Vannes[1], Victoria Margot Schlosser[1], Yusif Sarkis Yamin Albino[1], Parthasarathi Panda[2], Kalyan Kumar Sethi[2], Snehasis Jana[2, *]

[1]Trivedi Global, Inc., Henderson, USA

[2]Trivedi Science Research Laboratory Pvt. Ltd., Bhopal, India

Email address:

publication@trivedieffect.com (S. Jana)

[*]Corresponding author

To cite this article:

Mahendra Kumar Trivedi, Alice Branton, Dahryn Trivedi, Gopal Nayak, William Dean Plikerd, Peter L. Surguy, Robert John Kock, Rolando Baptista Piedad, Russell Phillip Callas, Sakina A. Ansari, Sandra Lee Barrett, Sara Friedman, Steven Lee Christie, Su-Mei Chen Liu, Susan Elizabeth Starling, Susan Jones, Susan Mardis Allen, Susanne Kathrin Wasmus, Terry Ann Benczik, Thomas Charles Slade, Thomas Orban, Victoria L. Vannes, Victoria Margot Schlosser, Yusif Sarkis Yamin Albino, Parthasarathi Panda, Kalyan Kumar Sethi, Snehasis Jana. A Systematic Study of the Biofield Energy Healing Treatment on Physicochemical, Thermal, Structural, and Behavioral Properties of Magnesium Gluconate. *International Journal of Bioorganic Chemistry*. Vol. 2, No. 3, 2017, pp. 135-145. doi: 10.11648/j.ijbc.20170203.19

Received: March 28, 2017; **Accepted**: April 7, 2017; **Published**: May 1, 2017

Abstract: Magnesium gluconate is a pharmaceutical/nutraceutical compound used as a source of magnesium ion. The recent study described the impact of The Trivedi Effect®-Energy of Consciousness Healing Treatment on magnesium gluconate for the variation in physicochemical, structural, thermal and behavioral properties using PXRD, PSD, FT-IR, UV-vis spectroscopy, TGA, and DSC analysis. Magnesium gluconate was divided into two parts – one part was control without any Biofield Energy Treatment, while another part was treated with The Trivedi Effect®-Energy of Consciousness Healing Treatment remotely by twenty renowned Biofield Energy Healers and defined as The Trivedi Effect® Treated sample. The PXRD analysis exhibited that the crystallite size of the treated sample was remarkably altered from -70% to 130% compared with the control sample. The average crystallite size was significantly decreased by 23.74% in the treated sample compared to the control sample. Biofield Energy Healing Treatment significantly reduced the particle size of magnesium gluconate at d10, d50, and d90 values by 12.15%, 8.98% and 15.35%, respectively compared to the control sample. The surface area analysis showed that surface area of the treated sample was significantly increased by 11.76% compared with the control sample. The FT-IR and UV-vis analysis displayed that structure of the magnesium gluconate persisted identical in both the treated and control samples. The TGA analysis exhibited four steps thermal degradation in both samples and the total weight loss of the Biofield Energy Treated sample was reduced by 0.19% compared with the control sample. The melting temperature of the Biofield Energy Treated sample (171.25ºC) was slightly (0.16%) higher from the control sample (170.97ºC). The latent heat of fusion was significantly decreased by 7.76% in the treated sample compared to the control sample. The TGA and DSC analysis revealed that the thermal stability of the treated sample was enhanced compared with the control sample. The current study revealed that The Trivedi Effect®-Energy of Consciousness Healing Treatment might produce a new polymorphic form of magnesium gluconate, which could be more soluble and bioavailable along with improved thermal stability compared with the untreated compound. The Biofield Treated sample could be more stable during manufacturing, delivery or storage conditions than the untreated sample. Hence, The Trivedi Effect® Treated magnesium gluconate would be very useful to design better nutraceutical/pharmaceutical formulations that might offer better therapeutic responses against inflammatory diseases, immunological disorders, stress, aging, and other chronic infections.

Keywords: Biofield Energy Healing Treatment, Consciousness Energy Healers, The Trivedi Effect®, Magnesium Gluconate, PXRD, Particle Size, TGA, DSC

1. Introduction

Magnesium gluconate is a classical nutraceutical/pharmaceutical compound as a source of magnesium ion, which is the vital element for more than 300 enzymes, DNA and RNA synthesis, reproduction and protein synthesis and also a vital coherent controller of glycolysis and the Krebs cycle in our body [1-3]. Magnesium gluconate is widely used for magnesium supplementation in hypomagnesemia. Magnesium gluconate is used for the prevention and treatment of several diseases, such as cancer, diabetes mellitus, allergies, septic shock, inflammatory diseases, immunological disorders, asthma, arrhythmias, acute myocardial infarction, gestational hypertension, preeclampsia, eclampsia, hearing loss, oxidative stress induced ischemia/reperfusion injury, etc. [4-10]. Magnesium gluconate can be used as an oral tocolytic agent [11], neuroprotective [12], and also used in a skin-tightening cosmetic composition [13]. Scientific literature demonstrated that magnesium gluconate is a potent antioxidant agent and is more physiologically acceptable salt with providing highest level of magnesium among the other commercially available magnesium salts such as chloride, sulfate, citrate, lactate, aspartate, etc. [4, 5, 14]. In this point of view, a novel proprietary herbomineral formulation was designed as a nutraceutical supplement, and can be used for the prevention and treatment of various human disorders. Magnesium gluconate is one of the components in this novel proprietary herbomineral formulation as the source of magnesium.

Since ancient times, many different cultures, religions, and systems of belief have recognized a living force that preserves and inhabits every living organism. This force is the source of 'life' and has been called various names, such as prana by the Hindus, *qi* or *chi* by the Chinese, and *ki* by the Japanese. This is believed to co-relate with the soul, spirit and mind. This hypothetical vital force has been scientifically evaluated and is now considered the Bioenergetics Field. The Biofield Energy is a dynamic electromagnetic field surrounding the human body, resulting from the continuous emission of low-level light, heat, and acoustical energy from the body. Biofield Energy is infinite, paradimensional and can freely flow between the human and environment [15]. Thus, a human has the ability to harness energy from the ionosphere of the earth, the "universal energy field", and transmit it to any living organism(s) or nonliving object(s) around the globe. The object or recipient always receives the energy and responds in a useful way. This process is known as The Trivedi Effect® - Biofield Energy Healing Treatment [16, 17]. Biofield (Putative Energy Field) based Energy Therapies are used worldwide to promote health and healing. The National Center of Complementary and Integrative Health (NCCIH) has recognized and accepted Biofield Energy Healing as a Complementary and Alternative Medicine (CAM) health care approach in addition to other therapies, medicines and practices such as natural products, deep breathing, yoga, Tai Chi, Qi Gong, chiropractic/osteopathic manipulation, meditation, massage, special diets, homeopathy, progressive relaxation, guided imagery, acupressure, acupuncture, relaxation techniques, hypnotherapy, healing touch, movement therapy, pilates, rolfing structural integration, mindfulness, Ayurvedic medicine, traditional Chinese herbs and medicines, naturopathy, essential oils, aromatherapy, Reiki, cranial sacral therapy and applied prayer (as is common in all religions, like Christianity, Hinduism, Buddhism and Judaism) [18]. Biofield Energy Healing Treatment (The Trivedi Effect®) has been published in numerous peer-reviewed science journals due to its significant impacts in the science fields of medical [19], biotechnology [20, 21], genetics [22, 23], microbiology [24-26], materials science [27, 28], agriculture [29, 30], pharmaceuticals [31, 32], nutraceuticals [33, 34], organic compounds [35, 36]. These publications reported that Biofield Energy Treatment (The Trivedi Effect®) has the significant capability to alter the physical, structural, chemical, thermal, and behavioral properties of the wide varieties of living and non-living substances. Although magnesium gluconate displayed highest bioavailability and moderate solubility in water in comparison to other magnesium salts, humans still face problems in achieving their daily requirements of magnesium [37]. The physical and chemical properties such as particle size, crystalline structure, crystallite size, surface area, etc. of a pharmaceutical have a direct influence on the absorption, dissolution, and bioavailability of the drug [38]. The stability of a solid drug with respect to the atmospheric conditions is very important to the pharmaceutical industry during processing, formulation, storage, and packaging in order to achieve better therapeutic efficacy [39]. Biofield Energy Treatment (The Trivedi Effect®) has been reported to change the particle size, specific surface area, crystalline, chemical and thermal behavior of an atom/ion through possible mediation of neutrinos [40]. Scientific literature mentions that powder X-ray diffraction (PXRD), particle size distribution analysis (PSD), Fourier transform infrared (FT-IR) spectrometry, ultraviolet-visible (UV-vis) spectroscopy, thermogravimetric analysis (TGA), and differential scanning calorimetry (DSC) analysis play an vital role for solving various problems encountered in industries for the pharmaceutical/nutraceutical formulation and developments [41]. By considering these aspects, the physicochemical, structural, thermal, and behavioral properties of the Biofield Energy Treated and untreated magnesium gluconate were studied using various analytical techniques including PXRD, PSD, FT-IR, UV-vis spectroscopy, TGA, and DSC.

2. Materials and Methods

2.1. Chemicals and Reagents

Magnesium gluconate hydrate was procured from Tokyo Chemical Industry Co., Ltd. (TCI), Japan. All other chemicals used in the experiment were of analytical grade available in India.

2.2. Energy of Consciousness Treatment Strategies

Magnesium gluconate was one of the components of the new proprietary herbomineral formulation, which was developed by our research team and was used *per se* as the test compound for the current study. The test compound was divided into two parts, one part of the test compound did not receive any sort of treatment and was defined as the untreated or control magnesium gluconate sample. The second part of the test compound was designated as the Biofield Energy Treated or The Trivedi Effect® Treated sample, which was received The Trivedi Effect®-Energy of Consciousness Healing Treatment (Biofield Energy Healing Treatment) by a group of twenty renowned Biofield Energy Healers remotely. Fifteen Biofield Energy Healers were remotely located in the U. S. A., two in Canada, one in the UK, one in Australia, and one in Germany. The test compound was located in the research laboratory of GVK Biosciences Pvt. Ltd., Hyderabad, India. The Trivedi Effect® - Energy of Consciousness Healing Treatment was provided for 5 minutes through the Healer's Unique Energy Transmission process remotely to the test compound, which was kept under laboratory conditions. None of the Biofield Energy Healers in this study visited the laboratory in person, nor had any contact with the compounds. Similarly, the control compound was subjected to "sham" healer for 5 minutes, under the same laboratory conditions. The sham healer did not have any knowledge about the Biofield Energy Treatment. After that, the Biofield Energy Treated and untreated samples were kept in similar sealed conditions and characterized thoroughly by PXRD, PSD, FT-IR, UV-visible spectroscopy, TGA, and DSC analysis.

2.3. Characterization

2.3.1. Powder X-ray Diffraction (PXRD) Analysis

The PXRD analysis was performed on PANalytical X'Pert Pro powder X-ray diffractometer system. The X-ray of wavelength of 1.54056 Å was used. The data was collected in the form of a chart of the Bragg angle (2θ) vs. intensity, and a detailed table containing information on peak intensity counts, d value (Å), relative intensity (%), full width half maximum (FWHM) (θ°). From the XRD results, the crystallite size (G) was calculated using X'Pert data collector and X'Pert high score plus processing software. The crystallite size (G) was calculated from the Scherrer equation [42, 43]. The method was based on the width of the diffraction patterns obtained in the X-ray reflected crystalline region. The crystallite size (G) was calculated by using the following formula 1:

$$G = k\lambda/(bCos\theta) \quad (1)$$

Where, k is the equipment constant (0.5), λ is the X-ray wavelength (0.154 nm); b in radians is the full-width at half of the peaks and θ is the corresponding Bragg angle.

Percent change in crystallite size (G) was calculated using the following equation 2:

$$\%\ \text{change in crystallite size} = \frac{[G_{\text{Treated}} - G_{\text{Control}}]}{G_{\text{Control}}} \times 100 \quad (2)$$

Where $G_{Control}$ and $G_{Treated}$ are the crystallite size of the control and Biofield Energy Treated samples, respectively.

A total of ~500.18 mg of the control and Biofield Energy Treated samples individually were used for the analysis and prepared by the back loading technique using the sample preparation kit. The sample was spread on the holder ring in sufficient quantity to fill the ring cavity. It was then pressed down using a powder press block and scrapped the powder that was in surplus using a glass slide in order to get a densely packed specimen. The bottom plate was placed onto the holder ring and clamped in position. The sample holder was then removed from the sample preparation table by turning it upside down. A smooth surface of the sample was obtained to ensure optimum results.

2.3.2. Particle Size Distribution (PSD) Analysis

The average particle size and particle size distribution were analyzed using Malvern Mastersizer 2000, UK, with a detection range from 0.01 µm to 3000 µm. The sample unit was filled with dispersant medium and operated the stirrer at 2500 rpm. Alignment of the optics was done and taken the background measurement. After the background measurement, the sample was added in to the sample unit with constant monitoring of the obscuration. When the obscuration of the sample reached in between 15% and 20%, further addition of the sample stopped. When the obscuration was stable, the measurement was taken twice and the average was taken of the two measurements. The average histogram of the two measurements was recorded. The printout of the average histogram of the two measurements were documented in this study. Along with histogram, the data was presented in a table format which includes particle size (µm). Also, the values at below 10% level (d_{10}), 50% level (d_{50}), and 90% level (d_{90}) were calculated from the histogram, and the calculations such as surface area (m^2/g) were done by using Mastersizer 2000 software. The percent change in particle size (d) for at below 10% level (d_{10}), 50% level (d_{50}), and 90% level (d_{90}) was calculated using the following equation 3:

$$\%\ \text{change in particle size} = \frac{[d_{\text{Treated}} - d_{\text{Control}}]}{d_{\text{Control}}} \times 100 \quad (3)$$

Where, $d_{Control}$ and $d_{Treated}$ are the particle size (µm) for at below 10% level (d_{10}), 50% level (d_{50}), and 90% level (d_{90}) of the control and Biofield Energy Treated samples, respectively.

The percent change in surface area (S) was calculated using the following equation 4:

$$\%\ \text{change in surface area} = \frac{[S_{\text{Treated}} - S_{\text{Control}}]}{S_{\text{Control}}} \times 100 \quad (4)$$

Where, $S_{Control}$ and $S_{Treated}$ are the surface area of the control and Biofield Energy Treated samples, respectively.

2.3.3. Fourier Transform Infrared (FT-IR) Spectroscopy

FT-IR spectroscopy of the magnesium gluconate was performed using Spectrum Two (Perkin Elmer, USA) Fourier Transform Infrared Spectrometer with the frequency range of 400-4000 cm^{-1} by using the pressed KBr disk technique.

2.3.4. Ultraviolet-Visible Spectroscopy (UV-Vis) Analysis

The UV-Vis spectral analysis was carried out using Shimadzu UV-2450 with UV Probe, Japan. The spectrum was recorded using 1 cm quartz cell with a slit width of 1.0 nm. The wavelength range chosen for recording the spectra was 190-800 nm. The absorbance spectra (in the range of 0.2 to 0.9) and absorbance maximum (λ_{max}) were recorded.

2.3.5. Thermal Gravimetric Analysis (TGA)

The TGA analysis was performed using TGA Q50 (TA Instruments, USA) at a heating rate of 10ºC/min from room temperature i.e. 25°C to 900°C in a nitrogen atmosphere. A total of ~15 mg of sample was weighed in a platinum crucible. In TGA, the weight loss for each step was recorded in grams as well as in percent loss with respect to the initial weight. Also, the onset, endset, and peak temperature for each step were recorded in TGA.

Percent change in weight loss (W) was calculated using the following equation 5:

$$\% \text{ change in weight loss} = \frac{[W_{Treated} - W_{Control}]}{W_{Control}} \times 100 \quad (5)$$

Where $W_{Control}$ and $W_{Treated}$ are the weight loss of the control and Biofield Energy Treated samples, respectively.

2.3.6. Differential Scanning Calorimetry (DSC)

Analysis was performed using the DSC Q20 (TA Instruments, USA) Differential Scanning Calorimeter. A total of ~8.23 mg of sample was weighed and sealed in an aluminum pan and equilibrated at 25 °C and heated up to 450ºC at the heating rate of 10ºC/min under nitrogen gas as purge atmosphere with the flow rate of 50 mL/min. The value for onset, endset, peak temperature, peak height (mJ or mW), peak area, and change in heat (J/g) for each peak were recorded.

The percent change in melting point (T) was calculated using the following equation 6:

$$\% \text{ change in melting point} = \frac{[T_{Treated} - T_{Control}]}{T_{Control}} \times 100 \quad (6)$$

Where, $T_{Control}$ and $T_{Treated}$ are the melting point of the control and Biofield Energy Treated samples, respectively.

The percent change in the latent heat of fusion (ΔH) was calculated using the following equation 7:

$$\% \text{ change in latent heat of fusion} = \frac{[\Delta H_{Treated} - \Delta H_{Control}]}{\Delta H_{Control}} \times 100 \quad (7)$$

Where $\Delta H_{Control}$ and $\Delta H_{Treated}$ are the latent heat of fusion of the control and Biofield Energy Treated samples, respectively.

3. Results and Discussions

3.1. Powder X-ray Diffraction (PXRD) Analysis

The PXRD diffractograms of both the control and Biofield Energy Treated magnesium gluconate are shown in Figure 1. The diffractograms exhibited sharp and intense peaks indicating that both the samples were crystalline in nature. PXRD data such as the Bragg angle (2θ), relative intensity (%), full width half maximum (FWHM) (θ°), and crystallite size (G) for the control and Biofield Energy Treated magnesium gluconate are presented in Table 1.

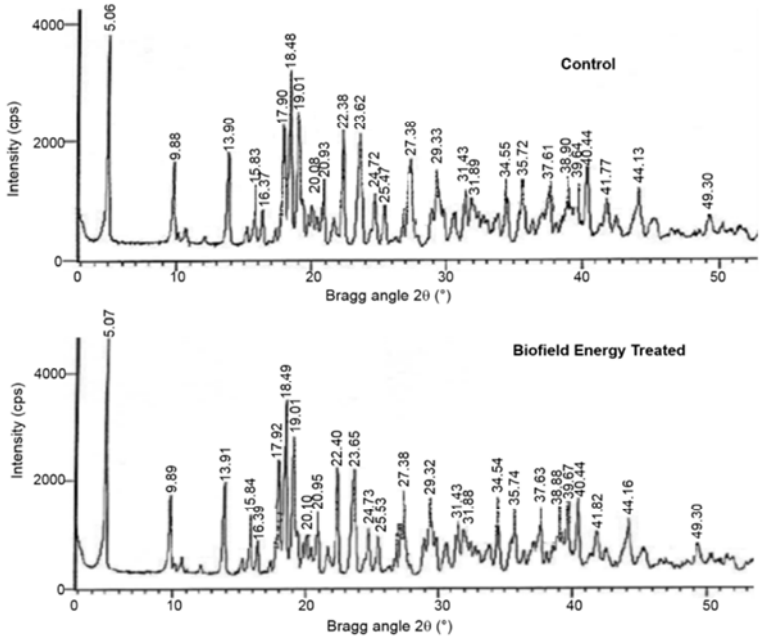

Figure 1. *Powder X-ray diffractograms of the control and Biofield Energy Treated magnesium gluconate.*

Table 1. *PXRD data for the control and Biofield Energy Treated magnesium gluconate.*

Entry No.	Bragg angle (°2θ)		Relative Intensity (%)		FWHM (°2θ)		Crystallite size (G, nm)		
	Control	Treated	Control	Treated	Control	Treated	Control	Treated	% change*
1	5.06	5.07	100.00	100.00	0.0836	0.0836	52.70	52.70	0.00
2	9.88	9.89	38.60	32.64	0.0836	0.1004	52.84	44.00	-16.73
3	13.90	13.91	39.88	35.20	0.1171	0.1338	37.87	33.14	-12.48
4	15.83	15.84	26.42	24.35	0.1338	0.1338	33.21	33.21	0.00
5	16.37	16.39	16.83	13.30	0.1004	0.1004	44.29	44.29	0.00
6	17.90	17.92	55.85	47.75	0.2175	0.1836	20.49	24.27	18.47
7	18.48	18.49	80.29	71.48	0.1171	0.1632	38.08	27.33	-28.25
8	19.01	19.01	65.26	53.17	0.1673	0.2448	26.68	18.23	-31.66
9	20.08	20.10	22.21	17.51	0.1506	0.1836	29.68	24.35	-17.97
10	20.93	20.95	29.75	24.34	0.1338	0.1632	33.45	27.43	-18.01
11	22.38	22.40	53.21	43.27	0.1673	0.2040	26.82	22.00	-17.99
12	23.62	23.65	49.88	40.37	0.1840	0.1632	24.44	27.56	12.75
13	24.72	24.73	23.84	17.44	0.0836	0.1428	53.90	31.56	-41.46
14	25.47	25.53	18.86	12.78	0.1338	0.1224	33.73	36.87	9.33
15	27.38	27.38	40.39	34.02	0.0669	0.2244	67.72	20.19	-70.19
16	29.33	29.32	36.46	28.83	0.0669	0.2040	68.02	22.31	-67.21
17	31.43	31.43	24.38	19.45	0.1673	0.1836	27.34	24.91	-8.88
18	31.89	31.88	22.16	17.34	0.1506	0.2040	30.40	22.44	-26.18
19	34.55	34.54	17.84	16.62	0.1004	0.1224	45.92	37.67	-17.98
20	35.72	35.74	31.36	25.34	0.1506	0.1836	30.71	25.19	-17.97
21	37.61	37.63	24.18	19.60	0.1171	0.1428	39.72	32.57	-17.99
22	38.90	38.88	20.20	15.07	0.1673	0.2040	27.91	22.89	-18.00
23	39.64	39.67	34.87	25.76	0.0669	0.1632	69.96	28.68	-59.00
24	40.44	40.44	35.83	31.18	0.0669	0.1020	70.13	46.00	-34.41
25	41.77	41.82	21.93	15.98	0.2007	0.3672	23.48	12.84	-45.33
26	44.13	44.16	26.20	21.11	0.2342	0.1020	20.29	46.58	129.63
27	49.30	49.30	15.20	10.46	0.1338	0.2040	36.21	23.75	-34.41
Average crystallite size							39.48	30.11	-23.74

FWHM: Full width half maximum, *denotes the percentage change in the crystallite size of the Biofield Energy Treated sample with respect to the control sample.

The crystallite size was calculated using Scherrer equation [42, 43]. The highest intense peak (100% relative intensity) in both the control and Biofield Energy Treated samples was observed at Bragg's angle (2θ) equal to 5.06 and 5.07°, respectively (Table 1, entry 1). Table 1 showed that 2θ of the both samples remained almost same in other XRD peaks, but the relative intensities of the peaks and crystallite size in the Biofield Energy Treated sample was found significantly different from the control sample. The crystallite sizes of the control and Biofield Energy Treated magnesium gluconate hydrate at position 2θ equal to nearly 5.1°, 15.8°, and 16.4° (Table 1, entry 1, 4, and 5) remained unchanged. Consequently, the crystallite size values of the Biofield Energy Treated sample at 2θ equal to nearly 9.88°, 13.9°, 18.5°, 19.0°, 20.1°, 20.9°, 22.4°, 24.7°, 27.4°, 29.3°, 31.4°, 31.9°, 34.5°, 35.7°, 37.6°, 38.9°, 39.6°, 40.4°, 41.8°, and 49.3° (Table 1, entry 2, 3, 7-11, 13, 15-25, and 27) were significantly decreased from 9% to 70% with respect to the control sample. Furthermore, the crystallite sizes of the control and Biofield Energy Treated magnesium gluconate at 2θ equal to nearly 17.9°, 23.6°, 25.5°, and 44.2° (Table 1, entry 6, 12, 14, and 26) were significantly increased from 9% to 130% in the Biofield Energy Treated sample in comparison to the control sample. The average particle size of the Biofield Energy Treated sample was significantly decreased by 23.74% compared to the control sample. Scientific literature reported that the changes in the XRD patterns, such as crystallite size and relative intensities, indicated the modification of the morphology of the crystal as well as the proof of polymorphic transition [44-46]. As the crystal morphology of the Biofield Energy Treated sample was altered compared with the control sample, the Biofield Energy Treated sample might be a new polymorphic form of magnesium gluconate. The crystal pattern, size and even polymorphic form of a pharmaceutical plays an important role in drug solubility, dissolution and bioavailability. It has been reported in the literature that the alteration in crystal morphology has significant impact on the in vitro dissolution rate, which is related with the bioavailability of orally administered pharmaceutical/nutraceutical [39]. Thus, it can be concluded that the Biofield Energy Healing Treatment might be a very useful method for enhancing the bioavailability of magnesium gluconate.

3.2. Particle Size Distribution (PSD) Analysis

The particle size values at $d_{10,}$ $d_{50,}$ and d_{90} values and surface area of both the control and Biofield Energy Treated magnesium gluconate were examined and the results are represented in Table 2.

Table 2. *Particle size data (d_{10}, d_{50}, and d_{90}) and surface area of the control and Biofield Energy Treated magnesium gluconate.*

Test Item	d_{10} (µm)	d_{50} (µm)	d_{90} (µm)	Surface area (m^2/g)
Control	7.16	43.00	189.09	0.34
Biofield Energy Treated	6.29	39.14	160.06	0.38
Percent change* (%)	-12.15	-8.98	-15.35	11.76

*denotes the percentage change in the particle size data (d_{10}, d_{50}, and d_{90}) and surface area of the Biofield Energy Treated sample with respect to the control sample.

The control sample showed a particle size values of d_{10} (7.16 µm), d_{50} (43.00 µm), and d_{90} (189.09 µm). After the Biofield Energy Healing Treatment, the particle size values of magnesium gluconate were found as 6.29, 39.14, and 160.06 µm for d_{10}, d_{50}, and d_{90}, respectively. Thus, Biofield Energy Treatment lowered significantly the particle size values of d_{10}, d_{50}, and d_{90} values of magnesium gluconate by 12.15%, 8.98% and 15.35%, respectively with respect to the control sample. The surface area analysis of both control and Biofield Energy Treated magnesium gluconate hydrate as shown in the Table 2 demonstrated that the surface area of the Biofield Energy Treated sample (0.38 m^2/g) was significantly increased by 11.76% from the control sample (0.34 m^2/g) as shown in Table 2.

Poorly crystallized compounds possess more surface area and higher exchange capacities than well-crystallized compounds [47]. In addition, the variation of the crystal morphology in the Biofield Energy Treated sample, which was well-supported from PXRD data, may cause to alter the surface area of the Biofield Energy Treated magnesium gluconate in comparison with the control sample. It has been well established that the particle size, shape and surface area of pharmaceutical compounds have an important impact on solubility, dissolution and in vivo bioavailability, as well as in helping the design of new drug delivery systems [48, 49]. Reduced particle size and higher surface area would increase the solubility of the solid particles, and consequently would improve the dissolution rate and bioavailability [50]. Thus, it is assumed that the Biofield Energy Treated magnesium gluconate might be dissolved and absorbed at a faster rate and may possibly have more bioavailability than normal magnesium gluconate.

3.3. Fourier Transform Infrared (FT-IR) Spectroscopy

The FT-IR spectra of both the control and Biofield Energy Treated magnesium gluconate shown in Figure 2, exhibited only one broad band with high intensity at 3398 cm^{-1}, which was attributed to the stretching vibrations of the hydroxyl groups originating from the water present in the magnesium gluconate. The bands of stretching vibrations of primary and secondary hydroxyl groups from the gluconate part of the compound appeared in this region. These bands were remained invisible due to the intensive broad band of water [51].

The FT-IR spectra of both the control and Biofield Energy Treated magnesium gluconate (Figure 2) demonstrated only one broad band centroid at 3398 cm^{-1}. This peak was attributed to the stretching vibrations of hydroxyl groups due to the water present in magnesium gluconate. The primary and secondary hydroxyl groups from the gluconate part of magnesium gluconate also showed the characteristic bands in this region that were remained undetectable due to the intensive broad band of water. The absorption peaks for the deformation vibration of the primary and secondary hydroxyl groups of the control sample were observed at 1434 cm^{-1} for in-the-plane δ(OH) and 636 and 578 cm^{-1} for the out-of-plane γ(OH), whereas these peaks were found in the spectrum of the Biofield Energy Treated sample at 1433, 636 and 577 cm^{-1}. The FT-IR spectra of both the control and Biofield Energy Treated samples exhibited C-H stretching at 2935 and 1381 cm^{-1}. A very sharp and intensive band at 1606 cm^{-1} for C=O stretching vibration of a carbonyl group of carboxylate anion was noticed in the spectra of both the control and Biofield Energy Treated samples. The band of the C-O stretching vibrations of the primary alcohol group was found at 1057 and 1056 cm^{-1} in the spectra of the control and Biofield Energy Treated sample, respectively. The absorption peaks at 1231 and 1142 cm^{-1} due to the C-O stretching vibrations of the secondary alcohol groups were observed in the spectrum of the control sample, whereas the Biofield Energy Treated sample showed these C-O stretching vibrations at 1231 and 1141 cm^{-1}. As there was no changes observed in the vibrational frequencies in both the control and Biofield Energy Treated samples, the structural properties of magnesium gluconate was remained unaltered after the Biofield Energy Healing Treatment.

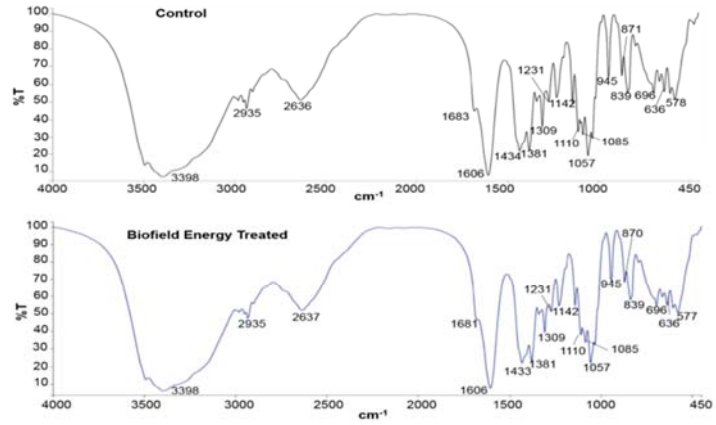

Figure 2. *FT-IR spectra of the control and Biofield Energy Treated magnesium gluconate.*

3.4. Ultraviolet-Visible Spectroscopy (UV-Vis) Analysis

Scientific literature described that 0.1% aqueous solution of magnesium gluconate showed a maximum absorption peak (λ_{max}) at 194.7 nm [52]. The UV-vis spectra of both the control and Biofield Energy Treated samples (Figure 3) displayed that the wavelength for the maximum absorbance (λ_{max}) of both the control and Biofield Energy Treated samples were at 198.0 nm and 198.6 nm, respectively with a minor shift of absorbance maxima from 2.2111 (control sample) to 2.2056 (Biofield Energy Treated sample).

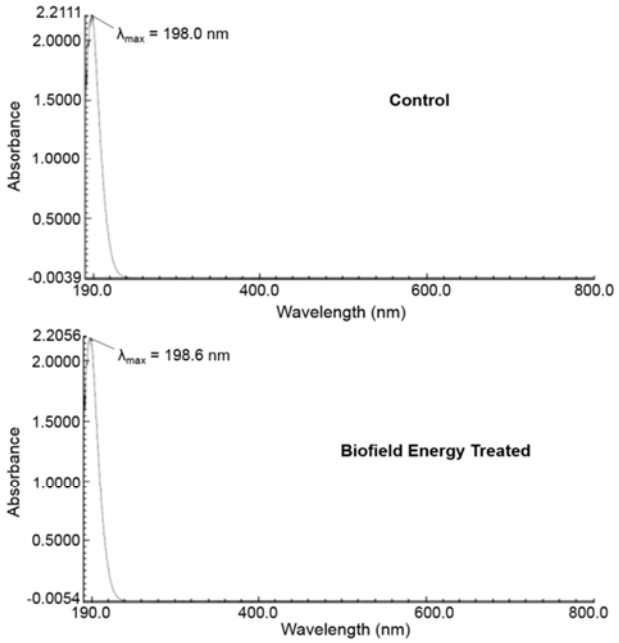

Figure 3. *UV-Vis spectra of the control and Biofield Energy Treated magnesium gluconate.*

The UV absorbance happens due to the different types of energy transitions from the singlet to the singlet excited state such as $\sigma \rightarrow \sigma^*, n \rightarrow \pi^*, and\ \pi \rightarrow \pi^*$. These types of electronic transitions are happened when the difference in energy between the lowest unoccupied molecular orbital (LUMO) and the highest occupied molecular orbital (HOMO) is significantly higher than the activation energy of the compound [53]. The λ_{max} of the Biofield Energy Treated sample was slightly (0.30%) higher than the control. It is then concluded that the structural configuration or activation energy of the Biofield Energy Treated sample was almost similar compared with the control sample.

3.5. Thermal Gravimetric Analysis (TGA)

The TGA and DSC are widely used analytical techniques for investigation of the thermal stabilities of pharmaceutical solids, determination of several kinetic parameters, and accomplishment of drug/excipient compatibility data for the pre-formulation study [54]. The TGA study of both the control and the Biofield Energy Treated magnesium gluconate (Figure 4) exhibited four thermal degradation steps and the data are presented in Table 3.

Table 3. *Thermal degradation steps of the control and Biofield Energy Treated magnesium gluconate.*

S. No.	Temperature (°C)		% Weight loss		% Change*
	Control	Treated	Control	Treated	
1st step of degradation	69.89	67.40	1.14	1.11	-2.63
2nd step of degradation	183.02	184.89	8.19	8.26	0.85
3rd step of degradation	301.13	300.51	38.79	38.77	-0.05
4th step of degradation	595.77	595.77	21.42	21.27	-0.70
Total weight loss	-	-	69.54	69.41	-0.19

*denotes the percentage change in the weight loss of the Biofield Energy Treated sample with respect to the control sample.

The weight loss of the Biofield Energy Treated sample at the first, second, and fourth steps of thermal degradation were decreased by 2.63%, 0.05%, and 0.70%, respectively compared to the control sample. Subsequently, the weight loss of the Biofield Energy Treated magnesium gluconate at the third step of degradation was increased by 0.85% compared to the control sample. The first step degradation was probably associated with the elimination of water in both the samples.

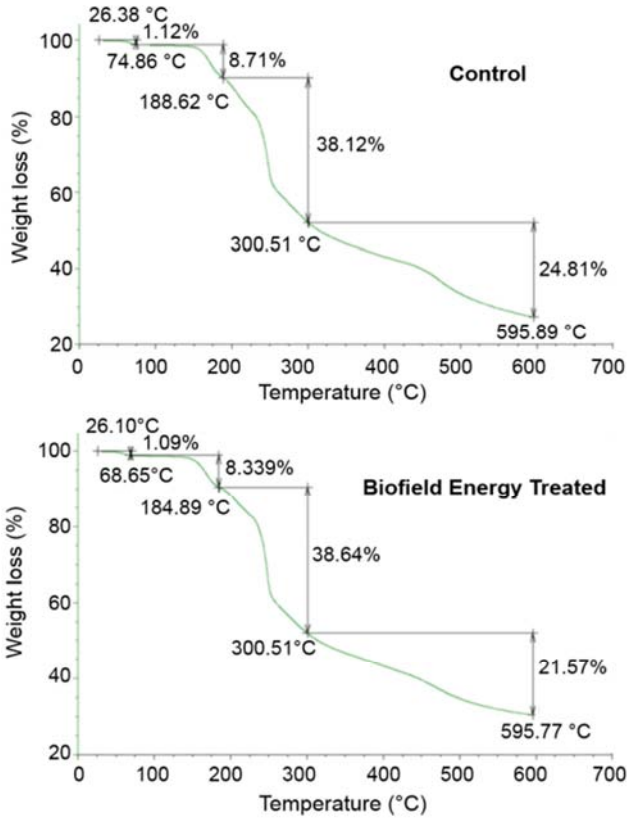

Figure 4. *TGA thermograms of the control and Biofield Energy Treated magnesium gluconate.*

The total weight loss was 69.54% and 69.41% in the control and Biofield Energy Treated samples, respectively from their initial weight from room temperature to 600°C (Table 3). Thus, the total weight loss of the Biofield Energy Treated sample was reduced by 0.19% compared with the control sample.

3.6. Differential Scanning Calorimetry (DSC) Analysis

The DSC thermograms of both the control and Biofield Energy Treated magnesium gluconate (Figure 5) showed two endothermic peaks. Their DSC data are presented in Table 4. The first broad endothermic (minor) peak was due to the removal of water from the sample. The second sharp endothermic (major) peak was due to the melting temperature of the magnesium gluconate.

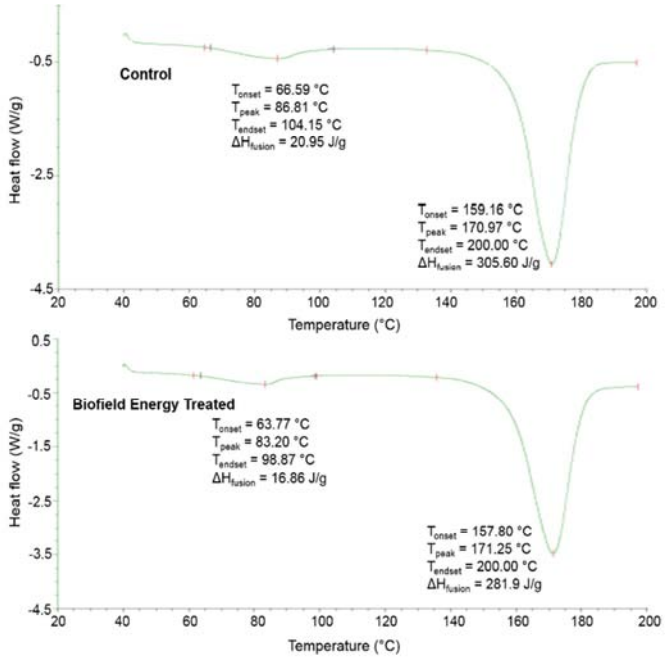

Figure 5. *DSC thermograms of the control and Biofield Energy Treated magnesium gluconate.*

The DSC data analysis (Table 4) revealed that the melting temperature of the Biofield Energy Treated sample (171.25ºC) was slightly (0.16%) higher from the control sample (170.97ºC). The latent heat of fusion in the Biofield Energy Treated magnesium gluconate was significantly decreased by 7.76% compared to the control sample (Table 4).

Table 4. *The latent heat of fusion (J/G) and melting point (°C) values of the control and Biofield Energy Treated magnesium gluconate.*

Endothermic peak	Description	T_{onset} (°C)	T_{peak} (°C)	T_{endset} (°C)	ΔH_{fusion} (J/g)
Minor peak	Control sample	66.59	86.81	104.15	20.95
	Biofield Treated sample	63.77	83.20	98.87	16.86
	% Change*	-4.23	-4.16	-5.07	-19.52
Major peak	Control sample	159.16	170.97	200.00	305.60
	Biofield Treated sample	157.80	171.25	200.00	281.90
	% Change*	-0.85	0.16	0.00	-7.76

T_{onset}: Onset melting temperature, T_{peak}: Peak melting temperature, T_{endset}: Endset melting temperature, ΔH: Latent heat of fusion, *denotes the percentage change of the Biofield Energy Treated sample with respect to the control sample.

Additionally, the temperature for water removal and the latent heat of fusion in the Biofield Energy Treated sample was significantly decreased by 4.16% and 19.52%, respectively compared with the control sample. Scientific literature reported that decreased particle size reduced the latent heat of fusion [55]. It is assumed that Biofield Energy Healing Treatment might lead to introduce enantiotropic form of magnesium gluconate. The Biofield Energy Treated sample, having a lower latent heat of fusion, would be a more stable and soluble polymorphic form at temperature below the transition point [45, 56].

4. Conclusions

The current analysis anticipated the significant effect of The Trivedi Effect®-Energy of Consciousness Healing Treatment (Biofield Energy Healing Treatment) on physicochemical, thermal and behavioral properties of magnesium gluconate. The PXRD analysis revealed that the crystallite size was significantly transformed from -70% to 130% in The Trivedi Effect® Treated magnesium gluconate compared to the control sample. The average crystallite size of the Biofield Energy Treated sample was significantly reduced by 23.74% compared with the control sample. Overall, the PXRD analysis showed that the crystal morphology of the Biofield Energy Treated sample was significantly changed compared to the control sample. PSD analysis revealed that the particle size of magnesium gluconate at d_{10}, d_{50}, and d_{90} values were significantly decreased by 12.15%, 8.98% and 15.35%, respectively in The Trivedi Effect® Treated sample compared to the control sample. The surface area analysis demonstrated that surface area of The Trivedi Effect® Treated sample was significantly enhanced by 11.76% compared with the control sample. The TGA analysis presented four steps thermal degradation of both the samples and the total weight loss was decreased by 0.19% in the Biofield Energy Treated sample compared with the control sample. The DSC analysis demonstrated that the melting temperature of the Biofield Energy Treated sample (171.25ºC) was slightly (0.16%) increased compared with the control sample (170.97ºC). The latent heat of fusion of the Biofield Energy Treated sample was significantly reduced by 7.76% compared to the control sample. The TGA and DSC analysis clearly indicated that the thermal stability of the Biofield Energy Treated sample was improved compared with the control sample. Thus, The Trivedi Effect® Treated magnesium gluconate would be a new polymorphic form of magnesium gluconate, which could be more soluble and bioavailable along with improved thermal stability compared with the untreated magnesium gluconate. Briefly, The Trivedi Effect® - Energy of Consciousness Healing Treatment could be a useful approach in the design of better nutraceutical and/or pharmaceutical formulations that can

offer significant therapeutic responses against various diseases such as diabetes, allergies, septic shock, sleep disorder, insomnia, anxiety, depression, Attention Deficit Disorder, Attention Deficit Hyperactive Disorder, mental restlessness (mind chattering), brain frog, low libido, impotency, lack of motivation, mood swings, fear of the future, confusion, migraines, headaches, forgetfulness, overwhelm, loneliness, worthlessness, indecisiveness, frustration, irritability, chronic fatigue, obsessive/compulsive behavior, panic attacks, Lupus, Systemic Lupus Erythematosus, Hashimoto Thyroiditis, Asthma, Chronic peptic ulcers, Tuberculosis, Hepatitis, Chronic active hepatitis, Celiac Disease (gluten-sensitive enteropathy), Addison Disease, Crohn's disease, Graves' Disease, Pernicious and Aplastic Anemia, Sjogren Syndrome, Irritable Bowel Syndrome (IBS), Multiple Sclerosis, arthritis, Chronic periodontitis, Ulcerative colitis, Chronic sinusitis, Myasthenia Gravis, Atherosclerosis, Vasculitis, Dermatitis, Diverticulitis, Alopecia Areata, Psoriasis, Scleroderma, Fibromyalgia, Chronic Fatigue Syndrome, Vitiligo, cardiovascular disease, cancer, Alzheimer's disease, dementia, cataracts, osteoporosis, hypertension, glaucoma, hearing loss, Parkinson's Disease, Huntington's Disease, Prion Disease, Motor Neurone Disease, Spinocerebellar Ataxia, Spinal muscular atrophy, Amyotrophic lateral sclerosis, Friedreich's Ataxia, Lewy Body Disease, chronic infections and many more.

Abbreviations

DSC: Differential scanning calorimetry, FT-IR: Fourier transform infrared spectroscopy, FWHM: Full width half maximum, G: Crystallite size, HOMO: Highest energy occupied molecular orbital, LUMO: Lowest energy unoccupied molecular orbital, TGA: Thermal gravimetric analysis, T_{onset}: Onset melting temperature, T_{peak}: Peak melting temperature, T_{endset}: Endset melting temperature, ΔH: Latent heat of fusion, UV-vis: Ultraviolet-visible spectroscopy, PSD: Particle size distribution; PXRD: Powder X-ray diffraction.

Acknowledgements

The authors are grateful to GVK Biosciences Pvt. Ltd., Trivedi Science, Trivedi Global, Inc., and Trivedi Master Wellness for their assistance and support during this work.

References

[1] Heaton FW (1990) Role of magnesium in enzyme systems in metal ions in biological systems, In: Sigel H, Sigel A (Eds.), Volume 26: Compendium on magnesium and its role in biology, nutrition and physiology, Marcel Dekker Inc., New York.

[2] Frick DN, Banik S, Rypma RS (2007) Role of divalent metal cations in ATP hydrolysis catalyzed by the hepatitis C virus NS3 helicase: Magnesium provides a bridge for ATP to fuel unwinding. J Mol Biol 365: 1017-1032.

[3] Garfinkel L, Garfinkel D (1985) Magnesium regulation of the glycolytic pathway and the enzymes involved. Magnesium 4: 60-72.

[4] Fleming TE, Mansmann Jr HC (1999) Methods and compositions for the prevention and treatment of diabetes mellitus. United States Patent 5871769, 1-10.

[5] Fleming TE, Mansmann Jr HC (1999) Methods and compositions for the prevention and treatment of immunological disorders, inflammatory diseases and infections. United States Patent 5939394, 1-11.

[6] Guerrera MP, Volpe SL, Mao JJ (2009) Therapeutic uses of magnesium. Am Fam Physician 80: 157-162.

[7] Gums JG (2004) Magnesium in cardiovascular and other disorders. Am J Health Syst Pharm 61: 1569-1576.

[8] Gröber U, Schmidt J, Kisters K (2015) Magnesium in prevention and therapy. Nutrients 7: 8199-8226.

[9] Clague JE, Edwards RH, Jackson MJ (1992) Intravenous magnesium loading in chronic fatigue syndrome. Lancet 340: 124-125.

[10] Weglicki WB (2000) Intravenous magnesium gluconate for treatment of conditions caused by excessive oxidative stress due to free radical distribution. United States Patent 6100297, 1-6.

[11] Martin RW, Martin JN Jr, Pryor JA, Gaddy DK, Wiser WL, Morrison JC (1988) Comparison of oral ritodrine and magnesium gluconate for ambulatory tocolysis. Am J Obstet Gynecol 158: 1440-1445.

[12] Turner RJ, Dasilva KW, O'Connor C, van den Heuvel C, Vink R (2004) Magnesium gluconate offers no more protection than magnesium sulphate following diffuse trau-matic braininjury in rats. J Am Coll Nutr 23: 541S-544S.

[13] Lee KH, Chung SH, Song JH, Yoon JS, Lee J, Jung MJ, Kim JH (2013) Cosmetic compositions for skin-tightening and method of skin-tightening using the same. United States Patent 8580741 B2.

[14] Coudray C, Rambeau M, Feillet-Coudray C, Gueux E, Tressol JC, Mazur A, Rayssiguier Y (2005) Study of magnesium bioavailability from ten organic and inorganic Mg salts in Mg-depleted rats using a stable isotope approach. Magnes Res 18: 215-223.

[15] Stenger VJ (1999) Bioenergetic fields. Sci Rev Alternative Med 3.

[16] Warber SL, Cornelio D, Straughn J, Kile G (2004) Biofield energy healing from the inside. J Altern Complement Med 10: 1107-1113.

[17] Rubik B (2002) The biofield hypothesis: Its biophysical basis and role in medicine. J Altern Complement Med 8: 703-717.

[18] Koithan M (2009) Introducing complementary and alternative therapies. J Nurse Pract 5: 18-20.

[19] Trivedi MK, Patil S, Shettigar H, Gangwar M, Jana S (2015) In vitro evaluation of biofield treatment on cancer biomarkers involved in endometrial and prostate cancer cell lines. J Cancer Sci Ther 7: 253-257.

[20] Trivedi MK, Patil S, Shettigar H, Bairwa K, Jana S (2015) Evaluation of phenotyping and genotyping characteristic of Shigella sonnei after biofield treatment. J Biotechnol Biomater 5: 196.

[21] Trivedi MK, Branton A, Trivedi D, Nayak G, Gangwar M, Jana S (2015) Bacterial identification using 16S rDNA gene sequencing and antibiogram analysis on biofield treated Pseudomonas fluorescens. Clin Med Biochemistry Open Access 1: 101.

[22] Trivedi MK, Branton A, Trivedi D, Nayak G, Gangwar M, Jana S (2015) Characterization of phenotype and genotype of biofield treated Enterobacter aerogenes. Transl Med 5: 155.

[23] Trivedi MK, Branton A, Trivedi D, Shettigar H, Nayak G, Mondal SC, Jana S (2015) Phenotyping and genotyping characterization of Proteus vulgaris after biofield treatment. International Journal of Genetics and Genomics 3: 66-73.

[24] Trivedi MK, Patil S, Shettigar H, Mondal SC, Jana S (2015) Evaluation of biofield modality on viral load of Hepatitis B and C viruses. J Antivir Antiretrovir 7: 083-088.

[25] Trivedi MK, Branton A, Trivedi D, Nayak G, Bairwa K, Jana S (2015) In vitro evaluation of antifungal sensitivity assay of biofield energy treated fungi. Fungal Genom Biol 5: 125.

[26] Trivedi MK, Patil S, Shettigar H, Gangwar M, Jana S (2015) Effect of biofield treatment on antimicrobials susceptibility pattern of Acinetobacter baumannii - An experimental study. J Clin Diagn Res 3: 1.

[27] Trivedi MK, Tallapragada RM, Branton A, Trivedi D, Nayak G, Latiyal O, Jana S (2015) Evaluation of physical and structural properties of biofield energy treated barium calcium tungsten oxide. Advances in Materials 4: 95-100.

[28] Trivedi MK, Nayak G, Patil S, Tallapragada RM, Latiyal O, Jana S (2015) Impact of biofield treatment on atomic and structural characteristics of barium titanate powder. Ind Eng Manage 4: 166.

[29] Trivedi MK, Branton A, Trivedi D, Nayak G, Mondal SC, Jana S (2015) Evaluation of biochemical marker - glutathione and DNA fingerprinting of biofield energy treated Oryza sativa. American Journal of BioScience 3: 243-248.

[30] Trivedi MK, Branton A, Trivedi D, Nayak G, Mondal SC, Jana S (2015) Morphological characterization, quality, yield and DNA fingerprinting of biofield energy treated alphonso mango (Mangifera indica L.). Journal of Food and Nutrition Sciences 3: 245-250.

[31] Trivedi MK, Branton A, Trivedi D, Shettigar H, Bairwa K, Jana S (2015) Fourier transform infrared and ultraviolet-visible spectroscopic characterization of biofield treated salicylic acid and sparfloxacin. Nat Prod Chem Res 3: 186.

[32] Trivedi MK, Branton A, Trivedi D, Nayak G, Bairwa K, Jana S (2015) Spectroscopic characterization of disulfiram and nicotinic acid after biofield treatment. J Anal Bioanal Tech 6: 265.

[33] Trivedi MK, Tallapragada RM, Branton A, Trivedi D, Nayak G, Latiyal O, Jana S (2015) Evaluation of biofield energy treatment on physical and thermal characteristics of selenium powder. Journal of Food and Nutrition Sciences. 3: 223-228.

[34] Trivedi MK, Tallapragada RM, Branton A, Trivedi D, Nayak G, Latiyal O, Mishra RK, Jana S (2015) Physicochemical characterization of biofield energy treated calcium carbonate powder. American Journal of Health Research 3: 368-375.

[35] Trivedi MK, Branton A, Trivedi D, Nayak G, Saikia G, Jana S (2015) chromatographic, spectroscopic, and thermal characterization of biofield energy treated N, N-dimethylformamide. American Journal of Applied Chemistry 3: 188-193.

[36] Trivedi MK, Branton A, Trivedi D, Nayak G, Saikia G, Jana S (2015) Characterization of physico-chemical and spectroscopic properties of biofield energy treated 4-bromoacetophenone. American Journal of Physical Chemistry 4: 30-37.

[37] Ranade VV, Somberg JC (2001) Bioavailability and pharmacokinetics of magnesium after administration of magnesium salts to humans. Am J Ther 8: 345-357.

[38] Chereson R (2009) Bioavailability, bioequivalence, and drug selection. In: Makoid CM, Vuchetich PJ, Banakar UV (eds) Basic pharmacokinetics (1st Edn) Pharmaceutical Press, London.

[39] Blagden N, de Matas M, Gavan PT, York P (2007) Crystal engineering of active pharmaceutical ingredients to improve solubility and dissolution rates. Adv Drug Deliv Rev 59: 617-630.

[40] Trivedi MK, Mohan TRR (2016) Biofield energy signals, energy transmission and neutrinos. American Journal of Modern Physics 5: 172-176.

[41] Chauhan A, Chauhan P (2014) Powder XRD technique and its applications in science and technology. J Anal Bioanal Tech 5: 212.

[42] Alexander L, Klug HP (1950) Determination of crystallite size with the X-Ray spectrometer. J App Phys 21: 137-142.

[43] Langford JI, Wilson AJC (1978) Scherrer after sixty years: A survey and some new results in the determination of crystallite size. J Appl Cryst 11: 102-113.

[44] Inoue M, Hirasawa I (2013) The relationship between crystal morphology and XRD peak intensity on $CaSO_4$. $2H_2O$. J Crystal Growth 380: 169-175.

[45] Raza K, Kumar P, Ratan S, Malik R, Arora S (2014) Polymorphism: The phenomenon affecting the performance of drugs. SOJ Pharm Pharm Sci 1: 10.

[46] Brittain HG (2009) Polymorphism in pharmaceutical solids in Drugs and Pharmaceutical Sciences, volume 192, 2nd Edn, Informa Healthcare USA, Inc., New York.

[47] Murray HH, Lyons SC (1960) Further correlation of kaolinite crystallinity with chemical and physical properties. Clays Clay Miner 8: 11-17.

[48] Sun J, Wang F, Sui Y, She Z, Zhai W, Wang C, Deng Y (2012) Effect of particle size on solubility, dissolution rate, and oral bioavailability: Evaluation using coenzyme Q_{10} as naked nanocrystals. Int J Nanomed 7: 5733-5744.

[49] Khadka P, Ro J, Kim H, Kim I, Kim JT, Kim H, Cho JM, Yun G, Lee J (2014) Pharmaceutical particle technologies: An approach to improve drug solubility, dissolution and bioavailability. Asian J Pharm Sci 9: 304-316.

[50] Buckton G, Beezer AE (1992) The relationship between particle size and solubility. Int J Pharmaceutics 82: R7-R10.

[51] Nikolic VD, Illic DP, Nikolic LB, Stanojevic LP, Cakic MD, Tacic AD, Ilic-Stojanovic SS (2014) The synthesis and characterization of iron (II) gluconate. Advanced Technologies 3: 16-24.

[52] Ji L, Yin W, Fu-Jia M (2004) Confirmation of the chemical structure of magnesium gluconate. Pharmaceutical Care and Research 4: 272-273.

[53] Hesse M, Meier H, Zeeh B (1997) Spectroscopic methods in organic chemistry, Georg Thieme Verlag Stuttgart, New York.

[54] Alves R, Reis TVS, Silva LCC, Storpírtis S, Mercuri LP, Matos JR (2010) Thermal behavior and decomposition kinetics of rifampicin polymorphs under isothermal and non-isothermal conditions. Braz J Pharm Sci 46: 343-351.

[55] Zhang M, Efremov MY, Schiettekatte F, Olson EA, Kwan AT, Lai SL, Wisleder T, Greene JE, Allen LH (2000) Size-dependent melting point depression of nanostructures: Nanocalorimetric measurements. Phys Rev B 62: 10548.

[56] Lee EH (2014) A practical guide to pharmaceutical polymorph screening & selection. Asian J Pharm Sci 9: 163-175.